Title

Comparison of Tissue Diffusion Measurements Using High-resolution and Standard Diffusion Tensor Imaging in Patients with Locally Advanced Breast Cancer

Author

Liu, Cheng-Liang

Publication Date

2012

Peer reviewed|Thesis/dissertation

Comparison of Tissue Diffusion Measurements Using High-resolution and Standard Diffusion Tensor Imaging in Patients with Locally Advanced Breast Cancer

by

Cheng-Liang Liu

THESIS

Submitted in partial satisfaction of the requirements for the degree of

MASTER OF SCIENCE

in

Biomedical Imaging

in the

GRADUATE DIVISION

DEDICATION

I dedicate this thesis to my family for nursing me with affections and love

&

the living memories of my grandparents.

ACKNOWLEDGMENTS

I am grateful to my advisor Dr. Nola Hylton for her invaluable guidance and constant encouragement. I express sincere gratitude to Dr. Ella Jones without whose support and suggestions this work would have been difficult. I would like to thank Dr. Lisa Wilmes for many engaging and interesting discussions. I specially thank Rebekah Mclaughlin for assisting my thesis writing enormously. I thank David Newitt and Evelyn Proctor who assisted a lot in this study.

Comparison of Tissue Diffusion Measurements Using High-resolution and Standard Diffusion Tensor Imaging in Patients with Locally Advanced Breast Cancer

Cheng-Liang Liu[1]

[1]UCSF Masters of Science in Biomedical Imaging Program, San Francisco, California

ABSTRACT

Objective: To evaluate fractional anisotropy (FA) in comparison to apparent diffusion coefficient (ADC) for discriminating between cancer and normal breast tissue using standard and high resolution diffusion tensor imaging (DTI).

Materials and Methods: Dynamic contrast enhanced MRI, standard DTI, and high-resolution DTI data were collected in ten patients with locally advanced breast cancer before the start of neoadjuvant treatment. Regions of interest were selected in tumor and ipsilateral normal tissue. ADC and FA values from both DTI sequences were calculated for tumor and normal tissue regions. Additional studies using an ice water phantom were performed to investigate the effects of off iso-center imaging location on quantitative diffusion measurements.

Results: ADC values computed from both standard and high-resolution DTI showed a significant difference between normal and tumor tissue ($p < 0.0001$). A statistically significant difference in FA value for normal and tumor tissue using high resolution DTI was also measured ($p = 0.02$). Standard DTI measurements of FA did not show a statistically significant difference. Estimates of ADC difference between normal and tumor tissue derived from high-resolution DTI were more accurate than those derived from standard DTI as reflected in narrower 95% confidence intervals. Phantom studies showed deviations of up to 16% (standard DTI) and 19% (high-resolution DTI) in ADC values and 44% (standard DTI) and 258% (high-resolution DTI) in FA values measured in left or right breast coil as off-center locations, as compared to measurements made using a head coil at the magnet iso-center.

Conclusions: Both standard and high-resolution DTI sequences found that tumor ADC is significantly lower than ADC of normal tissue. High-resolution DTI also showed that the FA value of tumor is significantly lower than normal tissue. High-resolution DTI sequence might be more sensitive and appears to give superior differentiation between normal tissue and cancer compared to standard DTI.

TABLE OF CONTENTS

LIST OF TABLES

LIST OF FIGURES

INTRODUCTION

Mammography, ultrasound, and magnetic resonance imaging (MRI) are the most commonly used modalities for breast imaging. Owing to its high sensitivity and exquisite spatial resolution, MRI has been recommended by the American College of Radiology for breast cancer screening in high-risk patients(1). Clinical MRI exams are performed using dynamic contrast enhanced (DCE) MRI techniques that acquire T1-weighted images before, during, and after injection of a gadolinium-based contrast agent. Breast cancer diagnosis is made on the basis of the degree and time course of signal intensity (SI) change in the first 1-2 minutes following contrast injection. A rapid and marked increase in SI, and the presence of signal washout after the initial phase, both increase the suspicion for cancer(2). The high resolution, three-dimensional format of MRI allows for accurate depiction of tumor extent. Indeed, MRI has been shown to be a better non-invasive tool for disease staging than other standard clinical practices(3-7). However, low specificity remains a limitation for breast MRI and prohibits its use as a routine diagnostic tool for breast cancer.

Diffusion techniques could potentially improve the specificity of MRI. Diffusion-weighted MR imaging (DWI) measures the apparent diffusion coefficient (ADC) of water movement and can differentiate the cellularity and microstructures of tumor from normal tissue. In fact, several studies have shown that low ADC values are linked to malignant breast tumors(8-13). Diffusion tensor imaging (DTI), which measures both ADC and fractional anisotropy (FA), also provides information for tissue characterization(14). While ADC provides a scalar magnitude measurement of water

movement, FA measures the directionality of water movement. DWI allows for the calculation of only ADC; whereas DTI can be used to measure both ADC and FA. Both diffusion measurements have potential for breast cancer characterization; previous results have shown that there are significantly lower ADC and FA values in breast cancers than normal breast tissue(10-13, 15).

The measurement of water movement by diffusion MRI provides structural information about tissue cellularity and microenvironment. Compared to normal tissue, tumors have more densely packed cells caused by sustained proliferative signaling, evasion of growth suppressors, resistance to cell death, and enabled replicative immortality(16). Lopez et al showed that mammary tumor tissue is stiffer than normal breast tissue due in part to increased tumor cellularity(17). As Figure 1 illustrates, the resulting lack of extracellular space in tumors decreases the diffusion or random movement of water molecules. This molecular diffusion is due to thermal energy, which causes molecules to propel themselves around their surrounding environment.

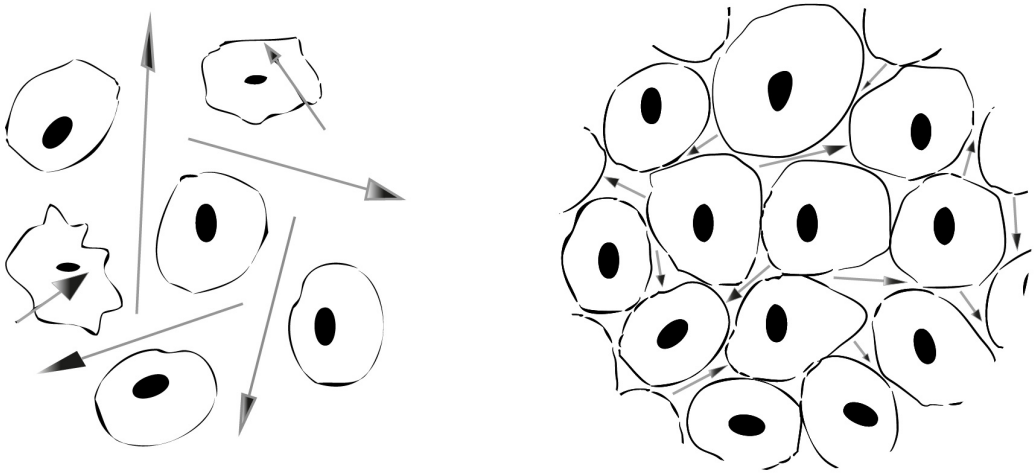

Figure 1. The images above illustrate the cellularity of normal tissue (left) and tumor (right). The arrows represent the possible directionality and magnitude of water movement in the extracellular space. Normal tissue cellularity has more extracellular space for water molecule movement than tumor tissue, as indicated by the more diverse pattern of arrows in the normal tissue (left) compared to the tumor tissue (right). The densely packed cellularity of the tumor restricts the water diffusion directionality and magnitude.

Consequently, tumor progression affects diffusivity of water molecules. Lopez et al also found that as normal mammary glands transitioned to invasive carcinoma, the tissue stiffened(17). This stiffening was partially caused by an increase in tumor epithelial cells, which decreased the extracellular space within the tumor. Thus, tumor progression led to decreased diffusivity of water molecules within the tumor.

In breast cancer diagnosis, an advantage of MRI is its high resolution compared to other imaging techniques. This is particularly important for demonstrating small and multi-centric disease. However, the voxel resolution of standard breast DTI is typically on the order of 3 mm^3, which is well below the standard resolution of contrast-enhanced breast

MRI. Improved DTI resolution is likely to provide better characterization of the microstructural properties of small and heterogeneous lesions. In addition, standard DTI has a long acquisition time and thus is more prone to image degradation from patient movement. Standard DWI has similar limitations as standard DTI. Thus, the goal of this project was to modify a high-resolution DWI sequence for high-resolution DTI and to apply this technique to the characterization of breast tumors(18). The high-resolution DWI sequence uses a two-dimensional (2D) echo-planar radiofrequency excitation pulse that simultaneously controls the slice and "slab" thickness, where the slab is the reduced field of view (FOV) direction during imaging(19). By using a 2D excitation pulse, we utilized a novel diffusion sequence with a reduced FOV (rFOV) in the phase encode direction. This sequence has the advantage of decreasing the number of k-space lines required to achieve a high-resolution image, while significantly reducing off-resonance induced artifacts with a shortened readout. It has the potential to reduce distortion by decreasing the required readout duration for imaging, and by allowing air-tissue interfaces to be excluded from the shim volume, it could also reduce susceptibility artifacts. Reducing the FOV can increase the resolution because the spatial domain and frequency domain are inversely proportional. If the FOV is reduced, the interval of each sampling point in k-space will increase. When the interval increases, the maximum range of the k-space also increases and thus decreases the pixel size in the space domain. To obtain diffusion tensor data, we acquired additional gradient directions, with a total of six directions.

Previous work found that high-resolution DWI improved image quality and tumor conspicuity compared to standard DWI. In addition, differences in tumor ADC values

indicated that there was less partial volume averaging with the smaller voxel size of the high-resolution technique(18). Therefore, we hypothesized that modifying the high-resolution technique to acquire a full diffusion tensor, might improve the sensitivity of FA information compared to standard DTI acquisition. The objective of this study was to compare the ADC and FA values of tumor and normal tissue from the high-resolution and standard DTI in patients with locally advanced breast cancer. Because the high-resolution DTI allows better distinction of the tumor boundary contour, the quantification of ADC and FA differences between tumor and normal breast tissue should be more conclusive than the standard DTI.

MATERIALS AND METHODS

Patient Eligibility

Fifteen patients with locally advanced breast cancer were enrolled in this retrospective study; all patients signed informed consent. All patients had pathology-confirmed invasive breast cancer and were scheduled to receive neoadjuvant chemotherapy. In order to be eligible for this study, DCE MRI, standard DTI, and high-resolution DTI data had to be collected in a single MRI exam before starting treatment.

Patient Imaging Acquisition

A 1.5 T GE Signa LX scanner (GE Healthcare, Waukesha, WI) with 40 mT/m maximum gradient strength and 150 mT/m/ms maximum slew rate was used to scan the patients. An eight-channel bilateral phased array breast coil (Hologic – formerly Sentinelle Medical, Toronto, Canada) was used to acquire data. A bilateral fat-suppressed T1-weighted DCE MRI was acquired using a three-dimensional fast gradient echo sequence. The DCE MRI scan time was between 80-100 sec, and scan collection continued for at least 8 min following contrast injection. Patients received 0.1 mmol/kg gadopentetate dimeglumine (Magnevist) contrast agent (Bayer Healthcase Pharmaceuticals, Berlin, Germany).

The DTI sequences were acquired following DCE imaging. The standard DTI images were acquired using an echo planar imaging sequence and the following parameters: TR/TE = 6000/69.6 ms, NEX = 6, matrix size = 128 × 128, slice thickness = 3 mm, pixel size = 3.125 × 3.125 mm^2. The high-resolution DTI protocol consisted of the previously referenced 2D spatially selective pulse, a 180° refocusing pulse for fat suppression, and the following parameters: TR/TE = 4000/72.8 ms, NEX = 10, matrix size = 128 × 64,

slice thickness = 4 mm, pixel size = 1.094 × 1.094 mm^2. Diffusion gradients were applied in six directions with b = 0 and 600 s/mm^2.

Phantom Study

MRI scanners are designed to have the highest homogeneity at the center of the instrument, which means the iso-center has a more uniform magnetic field than off-center areas. With good shimming, a high degree of uniformity enables chemically selective fat suppression. However, the bilateral coil elements for the breast coil are not located at the scanner's iso-center. In order to evaluate differences in diffusion measurements between iso-center and off-center locations, a phantom study was conducted. The phantom was comprised of two cylinders, with a smaller cylinder nested within a larger one as seen in Figure 2. This configuration creates two volumes: a central volume and an outer ring. A second, identical phantom was used in the opposite breast location.

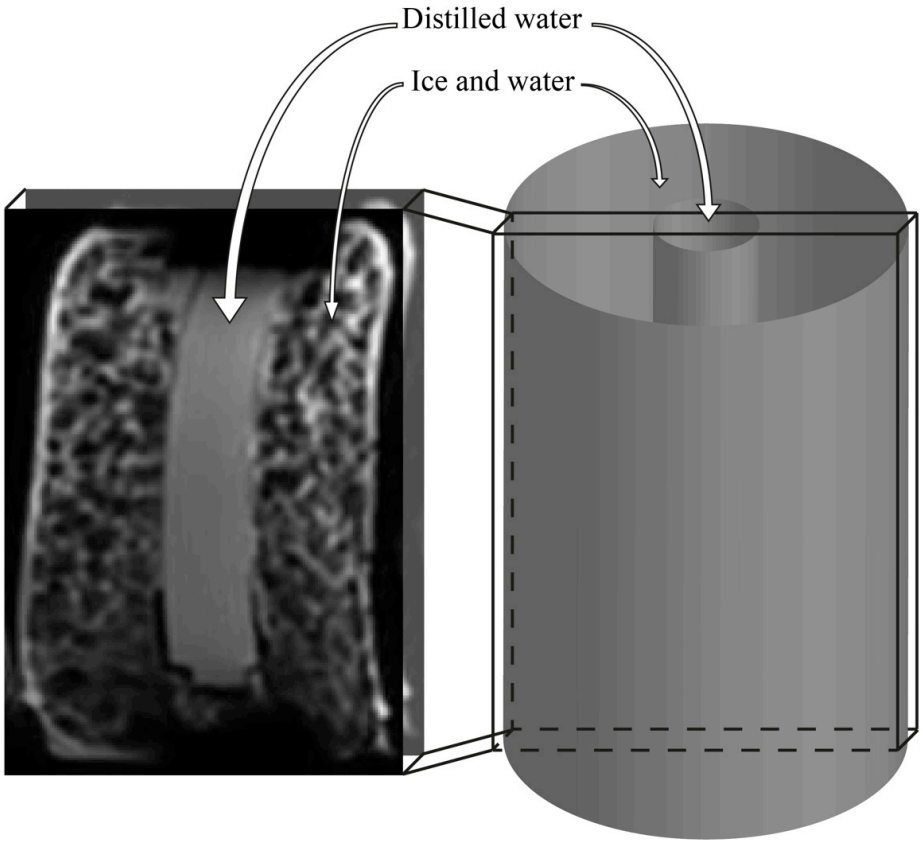

Figure 2. The phantom construction is shown above on the right. A representative T2-weighted MRI slice (left) illustrates the location of water and ice within the phantom. The central volume containing only water is seen as a uniform grey volume, whereas the outer ring volume appears mottled due to the mix of water and solid ice, which the MRI depicts as dark areas. The equilibrated ice and water in the outer ring ensures that the water in the central volume is maintained at 0°C.

For the first part of the study, the central volume of the phantom was filled with distilled water and the outer ring was filled with ice and water. The phantom was allowed to equilibrate for 50 min, ensuring that all water within the phantom was at 0°C. The DTI sequences were performed as detailed in the previous section on patient image acquisition.

In addition, the same DTI sequences were collected using the head coil as well as the breast coil. Because the ADC of water at 0°C is known and the head coil allows the phantom to be located in the scanner's iso-center, the phantom study in the head coil provided a reference value for comparison to the ADC values from the breast coil.

In the second part of the phantom study, the ADC value dependence on distance from the iso-center was further characterized. The central volume and outer ring of the phantom were filled with distilled water at room temperature, and DTI data was acquired in the breast coil only. The ADC was calculated for regions of interest (ROI) that covered not only left to right but also top to bottom in the water phantom, shown in Figure 3.

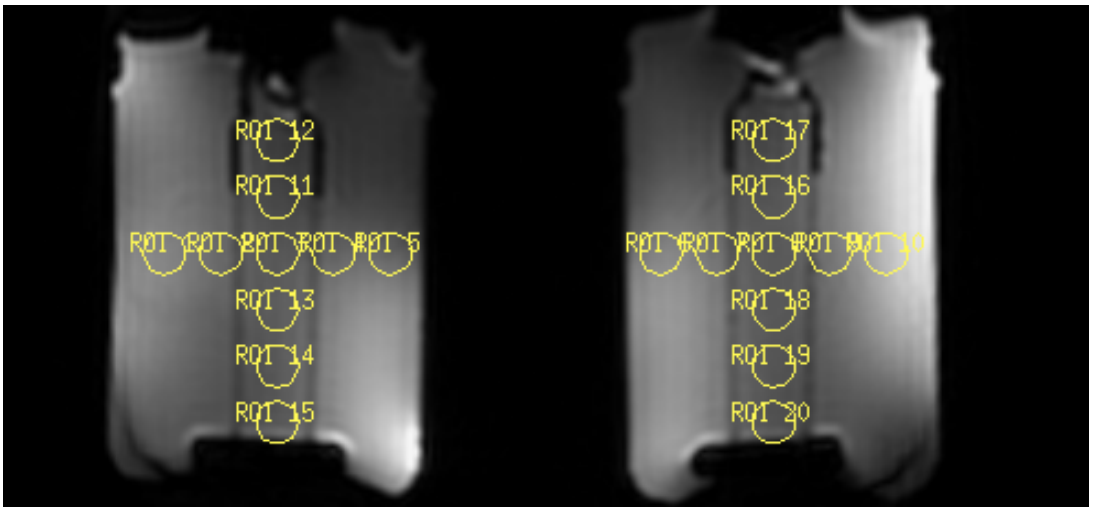

Figure 3. Shown above is the T2-weighted image of the two phantoms filled with room temperature water in the breast coil. The regions of interest (ROIs) are shown at multiple locations covering left to right and top to bottom.

MRI Diffusion Analysis

The diffusion gradient strength and time duration determine the b value. In a one-dimensional measurement, a bipolar gradient alters the signal intensity of diffusing water molecules by introducing phase differences that are proportional to the gradient strength. For non-moving spins, the equal lobes of the bipolar gradient produce a net phase difference of zero. However, if the water molecules are moving, the signal intensity will decrease because spins are incompletely rephased. The relationship between ADC and signal intensity is:

$$S_{after\ diffusion} = S_{before\ diffusion} \times e^{-b_{gradient}(ADC)}$$

We generated the rotationally invariant DTI parametric map, including the directionally averaged ADC and FA values, based on standard methods(20). The ADC value describes the degree of water mobility in tissue voxels, and is calculated with the following equation:

$$ADC = \frac{\lambda_1 + \lambda_2 + \lambda_3}{3}\ {mm^2}/{s}$$

where λ_1, λ_2, and λ_3 are the maximum, intermediate, and minimum diffusion tensor eigenvalues that describe the magnitude of diffusion along each of the three principal axes of the diffusion tensor ellipsoid, as seen in Figure 4.

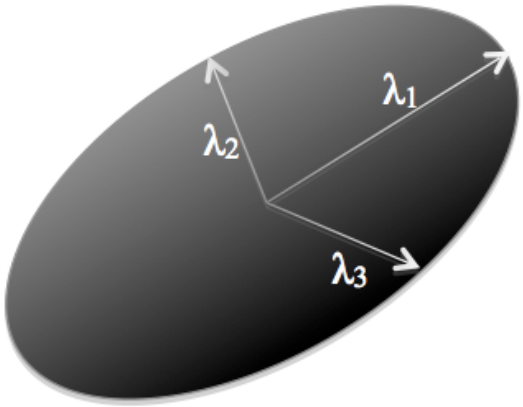

Figure 4. The three axes of the diffusion tensor ellipsoid are illustrated above by arrows. Three variables (λ_1, λ_2, λ_3) are assigned to the three axes to represent the magnitude of diffusivity along those axes of the diffusion tensor ellipsoid. The magnitude of diffusion along the longest axis is labeled λ_1, and the two remaining smaller axes are assigned the diffusivity variables λ_2 and λ_3.

In order to estimate the intra-voxel diffusivity, FA represents a unitless measure of the degree of directionality, which is calculated by:

$$FA = \frac{\sqrt{(\lambda_1 - \lambda_2)^2 + (\lambda_2 - \lambda_3)^2 + (\lambda_3 - \lambda_1)^2}}{\sqrt{2}\sqrt{{\lambda_1}^2 + {\lambda_2}^2 + {\lambda_3}^2}}$$

Diffusion behavior can vary from isotropic to highly anisotropic, reflecting differences in the microstructural properties of tissue. For isotropic diffusion, $\lambda_1 = \lambda_2 = \lambda_3$; for highly anisotropic diffusion, $\lambda_1 >> \lambda_2 \geq \lambda_3$. The former model has an FA value around zero. The latter model has a strongly preferred direction of diffusion, and the value of FA will be close to one.

Diffusion ROI Delineation

Lesions were identified as areas of contrast enhancement on the DCE MRI images. A tumor ROI was drawn manually to encompass the dark area on every slice of the ADC map that corresponded to the area of hyperintensity on the DCE MRI image. The tumor ROIs excluded any areas of vasculature, hematoma, necrosis, cyst, or image artifact. A second set of ROIs was manually drawn to include a region of normal appearing fibroglandular tissue in the ipsilateral breast. The normal fibroglandular ROIs excluded any areas that corresponded to abnormal enhancement on the DCE MRI. ROIs were drawn on the ADC map of the high-resolution DTI and then applied to the high-resolution DTI FA map and standard resolution DTI ADC map. If needed, the ROIs on the standard DTI ADC map were modified to better represent that image, and then applied to the standard DTI FA map. Thus, similar ROIs were used for tumor and normal tissue in the standard and high-resolution DTI, as seen in a representative patient in Figure 5.

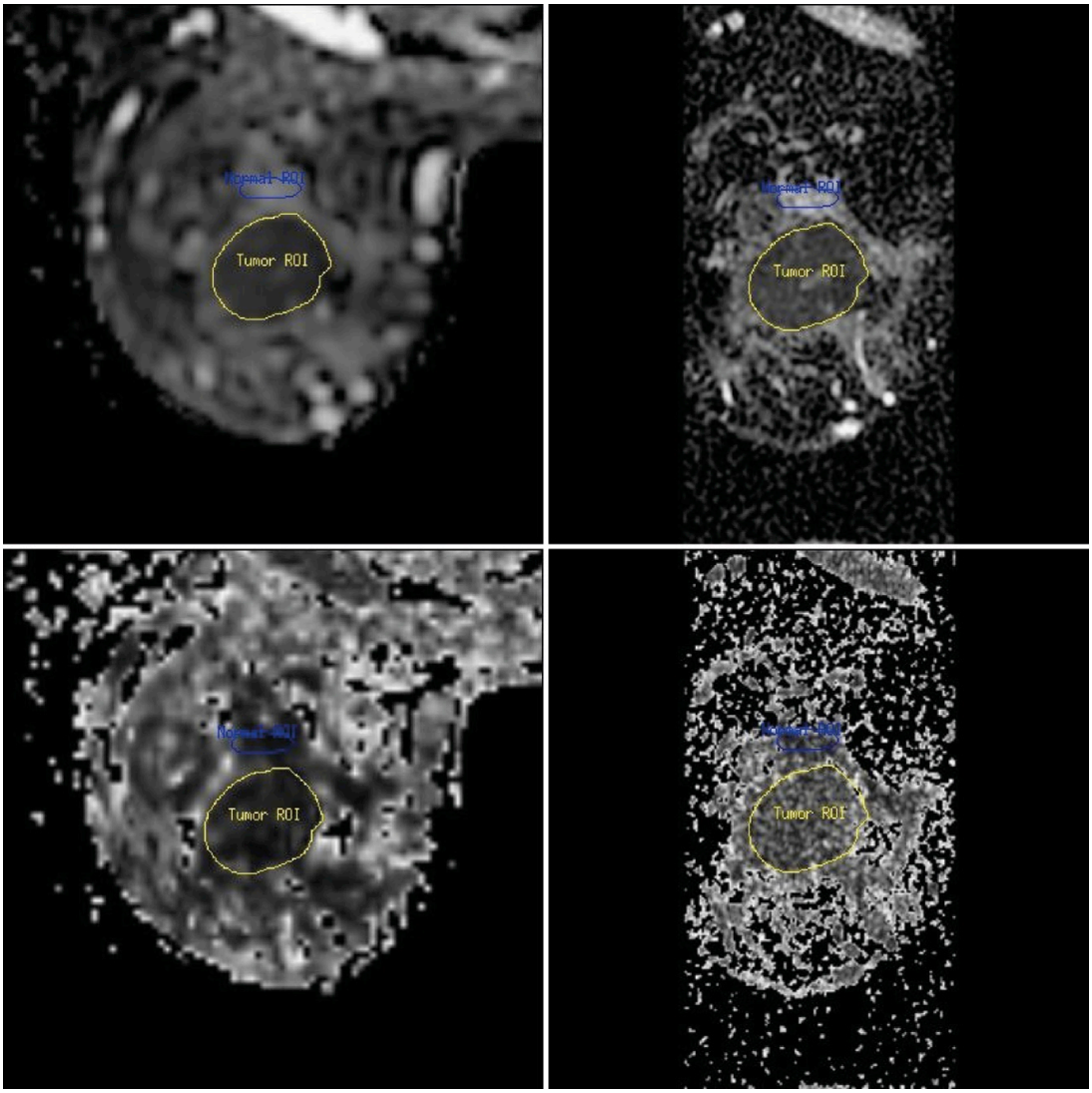

Figure 5. The image shows the tumor and fibroglandular ROIs on the standard DTI ADC (top left) and FA (bottom left) maps, as well as the high-resolution DTI ADC (top right) and FA (bottom right) maps. The tumor ROI is circled in yellow, and an area of normal tissue is circled in blue.

Statistical Analysis

The two-tailed paired Student's t-test was used to compare the ADC and FA data of tumor versus normal tissue in the same subjects for both standard and high resolution DTI sequences. Results are reported as mean differences, 95% confidence intervals (CI), and associated p-value for rejecting the null hypothesis of zero change between standard and high-resolution DTI results. A p-value ≤ 0.05 was considered statistically significant.

RESULTS

Patients Characteristics

Due to difficulty defining lesions, five cases were excluded from analysis. The remaining ten subjects ranged in age from 32 to 72 years old, with a mean of 47.3 years old. Their initial tumor volume, calculated by applying a 70% contrast enhanced threshold to the DCE MRI data(21), ranged from 0.185 to 4.68 cm^3, with a mean of 1.483 cm^3.

Phantom Data

Table I lists the ADC and FA values acquired in the phantom with water at 0°C. ADC values were 1.12×10^{-3} mm^2/s from both standard and high-resolution DTI sequences acquired in the head coil. ADC values varied from 1.20 to 1.33×10^{-3} mm^2/s in both sides of the breast coil for standard and high-resolution DTI. The off-center deviations of standard resolution DTI sequence up to 16% and high-resolution DTI sequence up to 19%. High-resolution DTI sequence had larger range of deviation than standard resolution DTI sequence.

Table I. Apparent diffusion coefficient (ADC) and fractional anisotropy (FA) in the ice water phantom from standard and high-resolution DTI sequences using the head and breast coil.

		Breast coil	
ADC (x 10^{-3} mm^2/s)	**Head coil**	Left	Right
Standard DTI	1.1207	1.2959	1.2834
High-resolution DTI	1.1185	1.3318	1.2029
		Breast coil	
FA	**Head coil**	Left	Right
Standard DTI	0.2202	0.2583	0.3168
High-resolution DTI	0.0627	0.1769	0.2243

The FA acquired in the head coil was 0.22 for standard DTI and 0.06 for high-resolution DTI. The standard DTI produced an FA value equal to 0.26 on the left side and 0.32 on the right side of the breast coil. The high-resolution DTI produced an FA value equal to 0.18 on the left side and 0.22 on the right side of the breast coil. The off-center deviations of standard resolution DTI sequence up to 44% and high-resolution DTI sequence up to 258%. In FA value comparison, high-resolution DTI sequence had larger range of deviation than standard resolution DTI sequence.

For the room temperature water phantom, both ADC and FA appeared lower in iso-center and gradually increased from center location to lateral sides. Figure 6 shows standard DTI ADC values of 2.6×10^{-3} mm^2/s on the far left to 2.2×10^{-3} mm^2/s in the center to 2.5×10^{-3} mm^2/s on the far right. High-resolution DTI produced ADC values from 2.2 to 2.3×10^{-3} mm^2/s on the left and from 1.9 to 2.2×10^{-3} mm^2/s on the right. ADC values in high-resolution DTI sequence were slightly lower than standard resolution DTI sequence.

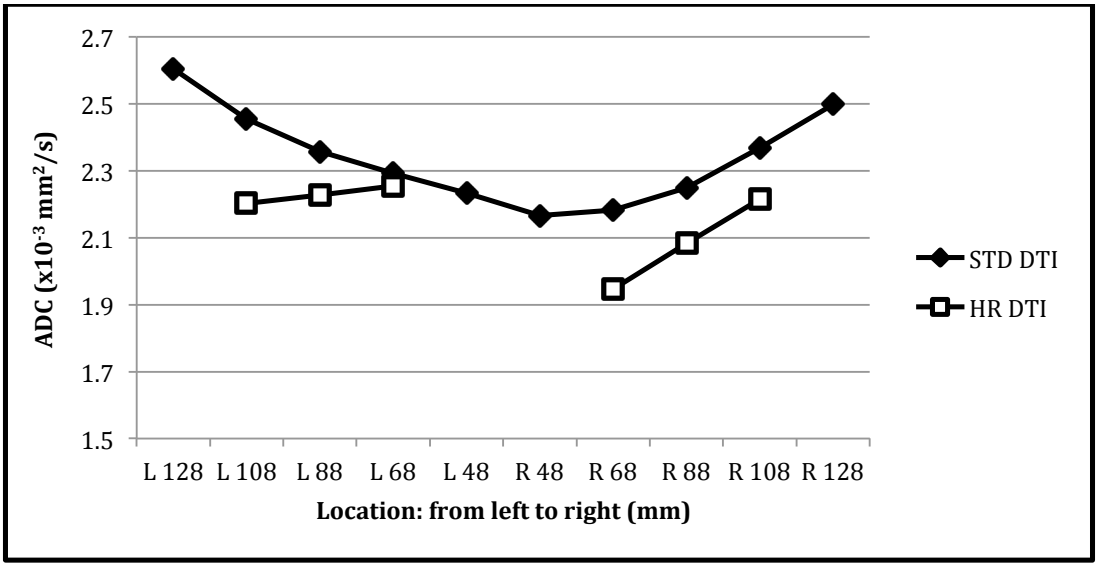

Figure 6. The graph shows the ADC values of room temperature water phantom at different locations in the breast coil. For standard DTI, the ADC value at the center was lower than at both lateral sides. For high-resolution DTI, the ADC values were similar on the left side, but right side values increased as the location proceeded further right.

Figure 7 shows standard DTI FA values of 0.19 on the far left to approximately 0.08 in the center to 0.27 on the far right. High-resolution DTI produced FA values from 0.34 to 0.23 on the left and from 0.26 to 0.41 on the right. High-resolution DTI sequence had higher FA values than standard resolution DTI sequence.

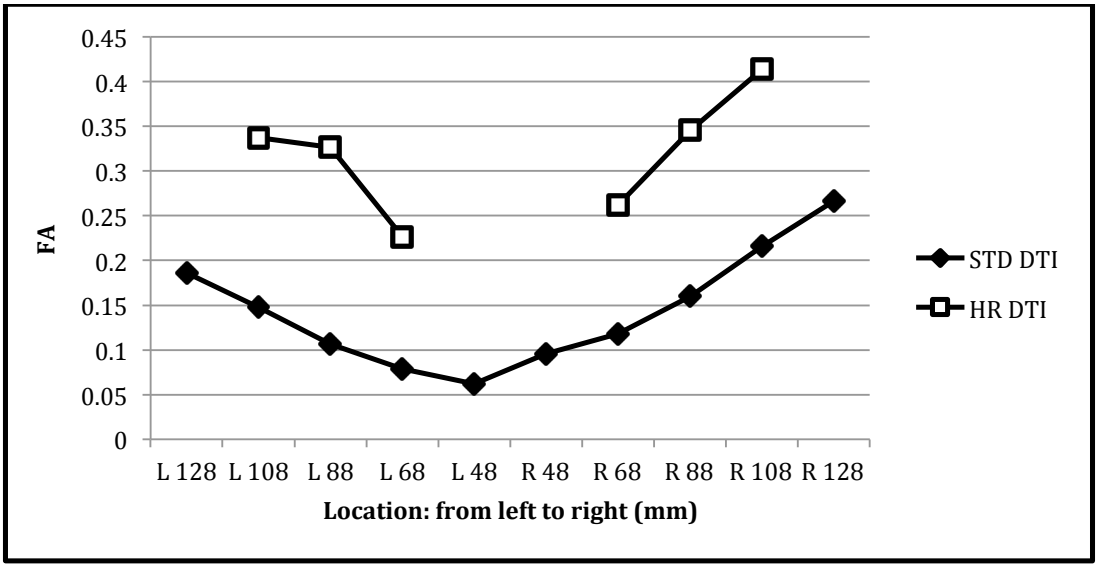

Figure 7. The graph shows the FA values of the room temperature water phantom at different locations in the breast coil. For standard DTI, the FA value at the center was lower than at both lateral sides. For high-resolution DTI, FA values were similarly elevated on the far lateral sides compared to more central locations.

Patient Analysis

Table II lists the ADC values calculated from standard and high-resolution DTI for normal and tumor tissue. The mean tumor ADC from standard DTI was 1.1750 ± 0.1809 × 10^{-3} mm^2/s compared to 2.0446 ± 0.1508 × 10^{-3} mm^2/s in normal tissue. The mean tumor ADC from high-resolution DTI was 1.1467 ± 0.1805 × 10^{-3} mm^2/s compared to 1.8932 ± 0.1674 × 10^{-3} mm^2/s in normal tissue.

Table III lists the FA values calculated from standard and high-resolution DTI for normal and tumor tissue. The mean tumor FA from standard DTI was 0.1724 ± 0.0455 compared to 0.1951 ± 0.0903 in normal tissue. The mean tumor FA from high-resolution DTI was 0.3100 ± 0.0785 compared to 0.3590 ± 0.0477 in normal tissue.

The results of the two tailed paired Student's t-test comparing tumor to normal appearing tissue can be seen in Table IV. The tumor and normal tissue ADC values were significantly different for standard DTI (mean difference = 0.8696, 95% CI = (0.7336, 1.0056), $p < 0.0001$) and high-resolution DTI (mean difference = 0.7464, 95% CI = (0.6146, 0.8782), $p < 0.0001$). For both standard and high-resolution DTI sequences, ADC values in tumor were lower than in normal appearing tissues. The tumor and normal tissue FA values were significantly different for high-resolution DTI (mean difference = 0.0491, 95% CI = (0.0115, 0.0867), $p = 0.0165$). Tumors' FA values were lower than normal appearing tissues' FA values in both standard and high-resolution DTI sequences. Only high resolution DTI sequence had significant lower FA values in tumor versus normal appearing tissue.

Table II. Apparent diffusion coefficient (ADC) values in patients from standard and high-resolution DTI sequences.

	Standard DTI ADC		**High-resolution DTI ADC**	
	Tumor	Normal	Tumor	Normal
Patient 1	1.0907	1.9839	1.0103	1.8502
Patient 2	1.1316	1.9125	1.0840	1.6626
Patient 3	1.1417	2.1981	1.0345	2.0343
Patient 4	0.8377	1.8768	0.8356	1.6816
Patient 5	1.4211	2.1211	1.4950	2.0539
Patient 6	1.3149	2.0077	1.2148	1.6999
Patient 7	1.4311	1.9886	1.2573	1.8290
Patient 8	1.1110	1.9387	1.0845	2.0521
Patient 9	1.0416	2.0420	1.2843	2.0432
Patient 10	1.2289	2.3767	1.1671	2.0252
Mean	1.1750 ± 0.1809	2.0446 ± 0.1508	1.1467 ± 0.1805	1.8932 ± 0.1674

The apparent diffusion coefficient (ADC) units for all values are $\times 10^{-3}$ mm^2/s.

Table III. Fractional anisotropy (FA) values in patients from standard and high-resolution DTI sequences.

	Standard DTI FA		**High-resolution DTI FA**	
	Tumor	Normal	Tumor	Normal
Patient 1	0.1468	0.1605	0.2838	0.3008
Patient 2	0.1282	0.1434	0.2480	0.3614
Patient 3	0.1674	0.1736	0.2372	0.3039
Patient 4	0.1898	0.1592	0.3079	0.3096
Patient 5	0.2854	0.4236	0.3020	0.3555
Patient 6	0.1672	0.2311	0.2297	0.3664
Patient 7	0.1347	0.1652	0.2431	0.3430
Patient 8	0.1796	0.2483	0.4160	0.4126
Patient 9	0.1374	0.1331	0.4374	0.4439
Patient 10	0.1871	0.1133	0.3944	0.3931
Mean	0.1724 ± 0.0455	0.1951 ± 0.0903	0.3100 ± 0.0785	0.3590 ± 0.0477

The fractional anisotropy (FA) is unitless value.

Table IV. The statistical results of the two tailed paired Student's t-test comparing apparent diffusion coefficient (ADC) and fractional anisotropy (FA) values of tumor versus ipsilateral normal appearing tissue from standard and high-resolution DTI.

	Two tailed paired Student's t-test		
ADC (x 10^{-3} mm^2/s)	Mean Difference	95% CI	p-value
Standard DTI	0.8696	(0.7336, 1.0056)	<0.0001 *
High-resolution DTI	0.7464	(0.6146, 0.8782)	<0.0001 *
	Two tailed paired Student's t-test		
FA	Mean Difference	95% CI	p-value
Standard DTI	0.0228	(-0.0190, 0.0646)	0.2478
High-resolution DTI	0.0491	(0.0115, 0.08670)	0.0165 *

95% CI indicates the 95% confidence interval.

DISCUSSION

The objective of this study was to compare the ADC and FA values of tumor and normal tissue from high-resolution and standard DTI studies in patients with locally advanced breast cancer. The mean ADC values for tumor and normal breast fibroglandular tissue calculated with both the standard and high-resolution DTI sequences were consistent with previous studies that found that tumor has lower ADC values than normal tissue(15). In addition, while ADC values from the standard and high-resolution DTI sequences were both significantly lower in tumor compared to normal tissue, the high-resolution DTI had a narrower 95% CI and thus provided a more accurate estimation of the difference.

FA values give additional information for differentiating tumor from normal tissue by characterizing the directionality of water movement. In this study, both DTI sequences found that tumor FA was lower than that of normal tissue FA. However, this difference was only significant for the high-resolution DTI sequence. The finding of a lower FA in tumor than normal tissues is in agreement with previous results(15).

However, there were limitations to this study. First, the results from the phantom studies indicate that both the ADC and FA values are affected by off-center location. The ADC values of the ice water phantom measured in the head coil were closer to the expected value of 1.1×10^{-3} mm^2/sec(22-25) than those measured by the breast coil. A similar result was found for FA of the ice water phantom; the FA values measured in the head coil were closer to zero, the expected value, than those measured in the breast coil. This effect is likely due to gradient non-linearity. To minimize its impact on the clinical study data, the tumor and normal tissue ROIs were taken from the same slice and in a similar position within the field of view.

In room temperature water phantom results, the ADC and FA values increased from the iso-center to the lateral sides in the standard resolution DTI sequence. This data indicates that gradient non-linearity affected the diffusion values at off-center locations more dramatically than at the iso-center. These off-center effects influenced high-resolution DTI sequence more exaggeratedly than standard resolution DTI sequence. It might be the fact that high-resolution DTI sequence was more sensitive to detect the differences. While this issue has not yet been addressed, repetition of the phantom study will allow the off-center effects to be measured and corrected, yielding more accurate ADC and FA values.

Another factor that may affect ADC and FA value is voxel anisotropy. In theory, a perfect cube is the optimal voxel for calculating the tensor. With an isotropic voxel, the directionality of water movement would be accurate and the exact FA value could be calculated. However, the high-resolution DTI used in this study has a spatial resolution of 1.094 × 1.094 x 4 mm, which is highly anisotropic. Future work will address this issue and an attempt will be made to implement a more isotropic voxel using the high-resolution DTI.

A major limitation of this study was the small sample size. With only 10 cases, the statistical tests performed on this data lacked power. However, the results of this study were very promising, and continued patient accrual will allow more robust statistical analysis in future studies. In addition, high-resolution DTI data will be collected as these patients undergo neoadjuvant chemotherapy, allowing future studies to investigate the relationship between diffusion measurements and treatment response.

CONCLUSIONS

Diffusion tensor imaging of breast cancer provides not only the magnitude of diffusivity but also water diffusion directionality. Tumor ADC values measured by both standard and high-resolution DTI were significantly lower than in normal tissue, consistent with previous findings. The high-resolution DTI derived tumor FA values were also significantly lower than those of normal fibroglandular breast tissue. These results support the hypothesis that high resolution DTI can improve discrimination between tumor tissue and normal tissue compared to standard DTI, and may provide a more detailed depiction of breast tissue microstructure.

REFERENCES

1. Lee CH, Dershaw DD, Kopans D, Evans P, Monsees B, Monticciolo D, Brenner RJ, et al. Breast cancer screening with imaging: Recommendations from the society of breast imaging and the ACR on the use of mammography, breast MRI, breast ultrasound, and other technologies for the detection of clinically occult breast cancer. (1558-349X (Electronic); 1546-1440 (Linking)).

2. Li X, Huang W, Rooney WD. Signal-to-noise ratio, contrast-to-noise ratio and pharmacokinetic modeling considerations in dynamic contrast-enhanced magnetic resonance imaging. (1873-5894 (Electronic); 0730-725X (Linking)).

3. Boetes C, Mus RD, Holland R, Barentsz JO, Strijk SP, Wobbes T, Hendriks JH, et al. Breast tumors: Comparative accuracy of MR imaging relative to mammography and US for demonstrating extent. (0033-8419 (Print); 0033-8419 (Linking)).

4. Kuhl CK, Schrading S, Weigel S, Nussle-Kugele K, Sittek H, Arand B, Morakkabati N, et al. [The "EVA" trial: Evaluation of the efficacy of diagnostic methods (mammography, ultrasound, MRI) in the secondary and tertiary prevention of familial breast cancer. preliminary results after the first half of the study period]. (1438-9029 (Print); 1438-9010 (Linking)).

5. Hillman BJ, Harms SE, Stevens G, Stough RG, Hollingsworth AB, Kozlowski KF, Moss LJ, et al. Diagnostic performance of a dedicated 1.5-T breast MR imaging system. (1527-1315 (Electronic); 0033-8419 (Linking)).

6. McLaughlin R, Hylton N. MRI in breast cancer therapy monitoring. (1099-1492 (Electronic); 0952-3480 (Linking)).

7. Lehman CD, Gatsonis C, Kuhl CK, Hendrick RE, Pisano ED, Hanna L, Peacock S, et al. MRI evaluation of the contralateral breast in women with recently diagnosed breast cancer. (1533-4406 (Electronic); 0028-4793 (Linking)).

8. Chen X, He XJ, Jin R, Guo YM, Zhao X, Kang HF, Mo LP, et al. Conspicuity of breast lesions at different b values on diffusion-weighted imaging. (1471-2407 (Electronic); 1471-2407 (Linking)).

9. Petralia G, Bonello L, Priolo F, Summers P, Bellomi M. Breast MR with special focus on DW-MRI and DCE-MRI. (1470-7330 (Electronic); 1470-7330 (Linking)).

10. Woodhams R, Matsunaga K, Kan S, Hata H, Ozaki M, Iwabuchi K, Kuranami M, et al. ADC mapping of benign and malignant breast tumors. (1347-3182 (Print); 1347-3182 (Linking)).

11. Guo Y, Cai YQ, Cai ZL, Gao YG, An NY, Ma L, Mahankali S, et al. Differentiation of clinically benign and malignant breast lesions using diffusion-weighted imaging. (1053-1807 (Print); 1053-1807 (Linking)).

12. Yoshikawa MI, Ohsumi S, Sugata S, Kataoka M, Takashima S, Kikuchi K, Mochizuki T, et al. Comparison of breast cancer detection by diffusion-weighted magnetic resonance imaging and mammography. (0288-2043 (Print); 0288-2043 (Linking)).

13. Park MJ, Cha ES, Kang BJ, Ihn YK, Baik JH. The role of diffusion-weighted imaging and the apparent diffusion coefficient (ADC) values for breast tumors. (1229-6929 (Print); 1229-6929 (Linking)).

14. Partridge SC, Murthy RS, Ziadloo A, White SW, Allison KH, Lehman CD. Diffusion tensor magnetic resonance imaging of the normal breast. (1873-5894 (Electronic); 0730-725X (Linking)).

15. Partridge SC, Ziadloo A, Murthy R, White SW, Peacock S, Eby PR, DeMartini WB, et al. Diffusion tensor MRI: Preliminary anisotropy measures and mapping of breast tumors. (1522-2586 (Electronic); 1053-1807 (Linking)).

16. Hanahan D, Weinberg RA. Hallmarks of cancer: The next generation. (1097-4172 (Electronic); 0092-8674 (Linking)).

17. Lopez JI, Kang I, You WK, McDonald DM, Weaver VM. In situ force mapping of mammary gland transformation. (1757-9708 (Electronic); 1757-9694 (Linking)).

18. Singer L, Wilmes LJ, Saritas EU, Shankaranarayanan A, Proctor E, Wisner DJ, Chang B, et al. High-resolution diffusion-weighted magnetic resonance imaging in patients with locally advanced breast cancer. (1878-4046 (Electronic); 1076-6332 (Linking)).

19. Saritas EU, Cunningham CH, Lee JH, Han ET, Nishimura DG. DWI of the spinal cord with reduced FOV single-shot EPI. (1522-2594 (Electronic); 0740-3194 (Linking)).

20. Basser PJ, Pierpaoli C. Microstructural and physiological features of tissues elucidated by quantitative-diffusion-tensor MRI. 1996. (1096-0856 (Electronic); 1090-7807 (Linking)).

21. Hylton NM. Vascularity assessment of breast lesions with gadolinium-enhanced MR imaging. (1064-9689 (Print); 1064-9689 (Linking)).

22. Mills E. Self-diffusion in normal and heavy water in the range 1-45.deg. Journal Physical Chemistry. 1973;77(5):685-8.

23. Simpson JH, Carr HY. Diffusion and nuclear spin relaxation in water. Phys Rev. 1958 09/01/;111(5):1201-2.

24. Krynicki K, Green CD, Sawyer DW. Pressure and temperature dependence of self-diffusion in water. Faraday Discuss Chem Soc. 1978;66:199-208.

25. Chenevert TL, Galban CJ, Ivancevic MK, Rohrer SE, Londy FJ, Kwee TC, Meyer CR, et al. Diffusion coefficient measurement using a temperature-controlled fluid for quality control in multicenter studies. (1522-2586 (Electronic); 1053-1807 (Linking)).

Publishing Agreement

It is the policy of the University to encourage the distribution of all theses, dissertations, and manuscripts. Copies of all UCSF theses, dissertations, and manuscripts will be routed to the library via the Graduate Division. The library will make all theses, dissertations, and manuscripts accessible to the public and will preserve these to the best of their abilities, in perpetuity.

Please sign the following statement:

I hereby grant permission to the Graduate Division of the University of California, San Francisco to release copies of my thesis, dissertation, or manuscript to the Campus Library to provide access and preservation, in whole or in part, in perpetuity.

Chengliang Liu
Author Signature

2012/09/08
Date